Chapter 7
Measurement of Sea Waves

Vincenzo Piscopo, Giovanni Battista Rossi, Francesco Crenna, Salvatore Gaglione, Antonio Scamardella, Marco Uttieri, and Enrico Zambianchi

Contents

Abstract This chapter focuses on the analysis and measurement of sea waves. After a brief review about the generation and propagation of ocean waves, the most common wave spectra are briefly described. Subsequently, the spectral analysis of sea waves is discussed focusing on the most promising techniques that allow obtaining the sea state parameters starting from the wave elevation time history. Finally, two techniques useful to measure the sea wave parameters are outlined. The former is based on the reverse analysis of the motions a ship advancing at a constant speed in a seaway, and the latter focuses on the employment of coastal high-frequency radars.

V. Piscopo (✉) · S. Gaglione · A. Scamardella · E. Zambianchi
Department of Science and Technology, University of Naples "Parthenope", Centro Direzionale, Isola C4, Naples, Italy
e-mail: vincenzo.piscopo@uniparthenope.it; salvatore.gaglione@uniparthenope.it; antonio.scamardella@uniparthenope.it; enrico.zambianchi@uniparthenope.it

G. B. Rossi · F. Crenna
Department of Mechanical, Energy, Management and Transportation Engineering, University of Genova, Genoa, Italy
e-mail: g.b.rossi@unige.it; francesco.crenna@unige.it

M. Uttieri
Department of Integrative Marine Ecology, Stazione Zoologica Anton Dohrn, Naples, Italy
e-mail: marco.uttieri@szn.it

P. Daponte et al. (eds.), *Measurement for the Sea*, Springer Series in Measurement Science and Technology,
https://doi.org/10.1007/978-3-030-82024-4_7

7.1 Modelling and Measuring of Sea Waves

7.1.1 Ocean Waves: A Brief Review

Ocean waves are generated by the interaction of wind and the water surface, based on two main physical processes, namely the friction between air and water and the local pressure field associated with the wind blowing over the wave surface [1]. In this respect, even if the mechanism that is on the basis of the energy transfer from wind to sea is not completely satisfactory, it is reasonable to assume that a storm wave system is the sum of many local interactions between wind and water distributed over space and time. Hence, during a storm, ocean waves grow with time depending on two main parameters, namely the fetch and duration. The former is the reference dimension of the storm area where the wind speed is steady, while the latter is the time interval between the storm inception and decay. Subsequently, ocean waves propagate from the storm area with a given celerity, depending on the water depth and the wavelength, namely the distance between two consecutive crests of the ocean wave. Indeed, if the wave amplitudes are small, if compared with the wavelength, the principle of linear superposition can be applied for the propagation and dispersion of the wave systems outside the storm area. In this respect, if wind speed is steady for a sufficiently long period and the fetch length is wide, ocean waves take on a stable structure, which is named fully developed sea state condition. On the contrary, if the fetch length or the storm duration is not sufficient to achieve a stable wave generation, the sea state condition is partly developed. The ocean waves inside the storm area are obtained by the superposition of a very large number of separate random and independent contributions, with different celerity and wavelength, that resemble a short-crested sea state condition. Anyway, as previously said, ocean waves propagate outside the storm area at different velocities, as longer waves travel faster than the shorter ones, producing at a great distance from the storm area a long-crested sea state condition, generally named swell.

In the last decades, a variety of theories have been developed to properly describe the wave kinematics [2]. The simplest and most applied wave model is the Airy theory, according to which the wave has the form of a sine curve and the free surface profile, representing the elevation as regards the undisturbed sea water level, is written in the following form:

$$\varsigma(t) = \varsigma_0 \cos\left[k\left(x - v_c t\right)\right] \tag{7.1}$$

where ς_0 is the wave amplitude, k is the wave number, connected to the wave celerity v_c by the equation $v_c^2 = g/k$ valid for the deepwater condition, and x is the distance of the measurement point, as regards a given reference system. The wave number and celerity are also connected to the wave circular frequency ω by the condition $\omega = kv_c$ valid for deepwater. Further details about the Airy wave theory are available in Ref. [1, 2].

7.1.2 Wave Spectra

Ocean waves are irregular and random in shape, height, length, and speed of propagation, so as they need to be described by random models based on frequency-dependent wave spectra, with given significant wave height, peak period, and shape function [3]. In this respect, real sea state conditions are generally obtained by the superposition of wind sea and swell components. The former is generated by local wind, while the latter has no relationship with the in situ met-ocean conditions and comes from areas located far from the measurement point.

The first pioneering studies on wave spectra were performed in the 50s by Neumann [4], Roll and Fisher [5], and Darbyshire [6] that developed the first frequency-dependent analytical formulations for single-peaked wave spectra. Nevertheless, these theoretical formulations are nowadays substantially unused as more refined wave spectra were developed for both fully and partly developed sea state conditions. Particularly, in 1964, Pierson-Moskowitz [7] provided a new analytical wave spectrum for fully developed wind seas, based on the analysis of a large amount of data collected in the Atlantic Ocean. The Pierson–Moskowitz (PM) wave spectrum S_{PM} is currently embodied for the design of ships and offshores structures, located in sea areas where fully developed sea state conditions are expected to occur as follows:

$$S_{PM}(\omega) = \frac{5}{16} H_s^2 \omega_p^4 \omega^{-5} \exp\left(-\frac{5}{4} \left(\frac{\omega}{\omega_p} \right)^{-4} \right) \tag{7.2}$$

having denoted by ω the circular wave frequency, by $\omega_p = 2\pi/T_p$ the spectral peak frequency depending, in turn, by the wave peak period T_p, and by H_s the significant wave height. In the subsequent years, an extensive wave measurement programme, also known as Joint North Sea Wave Project (JONSWAP), was carried out in the North Sea to derive a new analytical formulation, representative of wind-generated seas with limited fetch conditions. The JONSWAP spectrum S_J is currently formulated as a modification of the PM spectrum for a developing sea state in a fetch limited condition (7.3):

$$S_J(\omega) = A_\gamma S_{PM}(\omega) \gamma^{\exp\left(-0.5 \left(\frac{\omega - \omega_p}{\sigma \omega_p} \right)^2 \right)} \tag{7.3}$$

where γ is the nondimensional peak shape parameter, $A_\gamma = 1 - 0.287\ ln\ (\gamma)$ is the normalizing factor, and σ is the spectral width parameter, generally assumed equal to 0.07 and 0.09 if $\omega \leq \omega_p$ and $\omega > \omega_p$, respectively. The peak shape parameter mainly depends on the fetch length, and it is generally taken equal to 3.3 for the North Sea area. Besides, the condition $\gamma = 1$ resembles the fully developed sea state, corresponding to the PM wave spectrum. Fig. 7.1a reports a typical example of PM and JONSWAP spectra with H_s =4.0 m and T_p = 8.0 s.

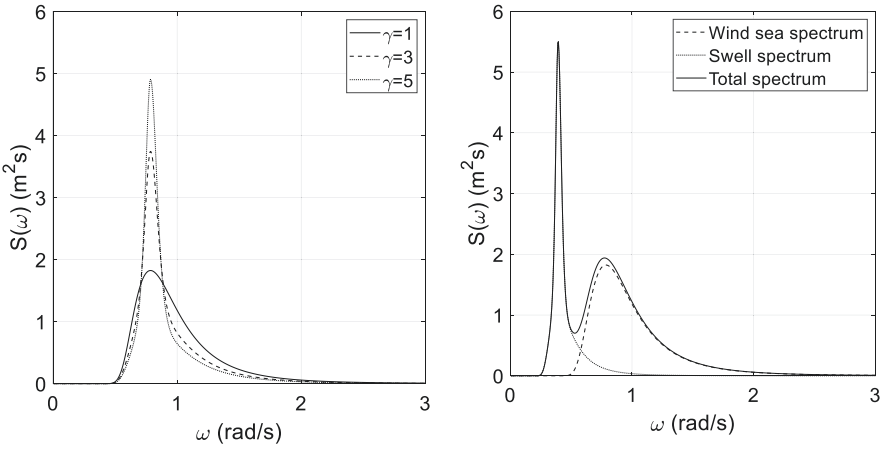

Fig. 7.1 Example of single-peak (**a**) and double-peak (**b**) spectra

In the same years, further studies were performed in order to develop theoretical models suitable for double-peaked wave spectra, obtained by combining wind sea and swell components. In this respect, in the 70s, Ochi and Hubble [8] provided a general spectral formulation, obtained as the sum of two gamma distributions, each one with the same three parameters of the JONWAP spectrum. Nevertheless, a simplified approach can be embodied, so as the double-peaked wave spectrum is regarded as the sum of two uncorrelated single-peaked wave spectra, representative of the wind sea S_{wind} and swell S_{swell} components, respectively, as follows:

$$S(\omega) = S_{\text{wind}}(\omega) + S_{\text{swell}}(\omega) \tag{7.4}$$

In Eq. (7.4), the wind sea spectrum is generally described by Eq. (7.2 and 7.3), while the swell component can be described by either a generalized JONSWAP spectrum or a normal function [9]. Figure 7.1b provides an example of double-peaked wave spectrum. The wind sea component has the same values as the fully developed PM spectrum depicted in Fig. 7.1a, while the swell spectrum is characterized by the following values: H_s =3.0 m and T_p = 16.0 s and γ = 5.0. By Fig. 7.1b, it is gathered that the swell component is generally much more peaked if compared with the wind sea one, as it is representative of past storm conditions, located quite far from the measurement point. Assuming a specific spectrum, sea wave observation can be simulated by generating times series in agreement with assumed spectrum, according to:

$$\varsigma(t) = \sum_{i=1}^{n} \sqrt{2S(f_i)df_i}\cos\left[2\pi f_i t + \varphi_i\right] \tag{7.5}$$

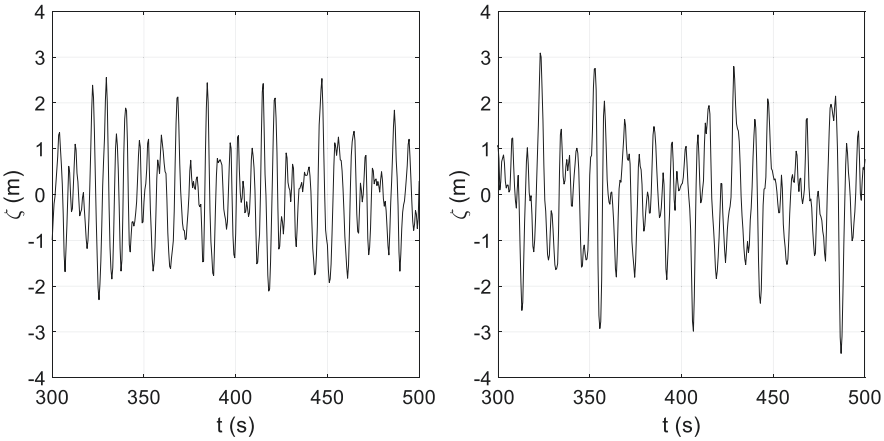

Fig. 7.2 Simulated sea wave elevation for the spectra of Fig. 7.1a, b

after partitioning the theoretical wave spectrum into a discrete set of components. In Eq. (7.5), ς denotes the wave amplitude, while f_i is the ith wave frequency component, with uniform random phase φ_i in the interval $[0,2\pi]$. Example of simulated time series, corresponding to the spectra depicted in Fig. 7.1, is shown in Fig. 7.2. In the case of Fig. 7.2b, the presence of low-frequency components, related to the swell phenomenon, can be noted.

7.1.3 Sea Wave Monitoring Techniques

Different sea wave monitoring techniques are available to measure the wave elevation and monitor the sea state condition. The most applied method involves the wave buoys that are generally connected in a network, whose working principle has been discussed in Chap. 2. Besides, different techniques are available to measure the sea state condition. Particularly, the two different techniques are discussed, in Subsections 7.3 and 7.4, respectively. The former is based on a reverse analysis technique of the motion of a floating buoy, namely a ship, which advances at a constant speed in a seaway. The latter instead involves one of more high-frequency wave radars, generally located along the coastline or, in some cases, being part of the measurement system installed onboard a ship.

7.2 Spectral Analysis of Sea Waves

7.2.1 Spectrum Estimation

Once an elevation record has been obtained, for example, by an inertial sensor mounted on a wave buoy, the useful information is best expressed by the estimated wave spectrum or by the estimated sea state parameters. Since the latter are typically obtained by the spectrum, spectrum estimation plays a key role in wave monitoring.

Along the years, several estimation methods have been proposed that can be parsed in two main groups, namely nonparametrical and parametrical [10]. The seminal idea under the first group was Schuster's "periodogram" [11], that is, the square of the Fourier transform (FT) of the series of observations, normalized in respect of the observation duration, T_0. Originally proposed for identified hidden periodicities in noisy signals, the periodogram constitutes a rough estimate of the power spectral density (PSD), since it is both biased and it has a large variance that does not decrease even by increasing the observation time. Yet, the basic periodogram can be improved both to reduce bias, which is usually accomplished by data tapering or prewhitening, and by reducing variance, by averaging in the time domain or smoothing in the frequency domain. An important method that moves along these lines was proposed by Welch [12] that will be discussed in the following.

Another important method was proposed by Thomson [13], whose basic idea was to taper the data with an orthonormal series of tapers, each of which highlighting different and complementary aspects of the signal, hence denomination of multitaper method (MTM).

Lastly, an approach alternative to the above nonparametrical methods is called parametrical and consists of considering parametrical models of the observed time series, such as the autoregressive (AR) or the autoregressive-moving average (ARMA) ones [14]. Once such a model has been fitted to the observations, the PSD can be obtained analytically. For brevity, we will not deal with these methods here.

Let us now discuss Welch's method in greater detail. The first step of the analysis procedure consists in parsing the overall data record, having an observation duration T, in n smaller segments of duration T_0, with partial overlap, typically from 20% to 50%. Each segment is pretreated by multiplying it by a smooth observation window, to limit the edge effect due to the *cutting* of the time series at the edges of the segment. (Such effect consists, in the spectral domain, in some *spectral leakage*. This effect can be simply described as follows. Consider a discrete spectrum: in consequence of the sharp truncation of the signal at the edges of the considered segment, part of the energy associated with each spectral component spreads around that component, causing not only an inexact estimation of the energy associated with it, but also some smearing of the components close to it, which is even more annoying. For a continuous spectrum, the effect is similar. Since this is an edge effect, it is intuitive that tapering can reduce it since it weights decreasingly data as long as they approach the edges.) Then, for each segment, the (modified) periodogram is

calculated and the spectrum is finally obtained by averaging over such periodograms. Therefore, spectral leakage is reduced by tapering and variance is reduced by averaging. Let us now consider the procedure in greater detail. Let us then denote the series of measurements by $x_i = x(i\Delta t)$, where Δt is the sampling interval, and $i = 1, \ldots N$, with $T = N\Delta t$, and $T_0 = N_0\Delta t$. Let $w_1,\ldots,w_{N_0}$ be a data taper, then the modified periodogram for the l th segment is as follows:

$$\hat{S}_l(f) = \Delta t \left| \sum_{i=1}^{N_0} w_i x_{i+l-1} e^{-j2\pi fi\Delta t} \right|^2 \tag{7.6}$$

where j is the imaginary unit. The spectral estimator is then:

$$\hat{S}(f) = \frac{1}{n} \sum_{k=0}^{n-1} \hat{S}_{km+1}(f) \tag{7.7}$$

where n is the number of segments and m is an integer-valued shift factor, satisfying $0 < m \leq N_0$ and $m(n-1) = N - N_0$.

To apply the method, a proper choice of the analysis features is required. The total observation time, T, is typically fixed by general experimentation constraint. The remaining features include the kind of taper, the degree of overlap, and the duration of individual segments, T_0. The goal is to optimize the main "metrological" characteristics of the method, namely its spectral resolution and its variance, or standard deviation. The spectral resolution can be understood as the capability of properly representing spectral components, i.e., peaks or, more generally, local maxima, in terms of localization of the peak/maximum and of restitution of its bandwidth. Spectral resolution is (inversely) related to the effective bandwidth, in that a large effective bandwidth implies a poor spectral resolution. Variance instead is a measure of statistical (in)stability. More practical a high variance results in a "noisy" spectrum. For example, in the spectrum of Fig. 7.2, there are two peaks, physically corresponding to the two superimposed sea states, the swell peak is narrowband, and the wind one is broadband. Spectral resolution will be more critical for the former, variance for the latter. Coming back to Welch's method, the choice of the degree of overlap is related to the kind of taper adopted, in that the smoother the taper is, the higher the degree of overlap can be adopted, which results in a larger number of segments, with a reduction of the variance. On the other hand, the smoother the window is, the larger its bandwidth is and, consequently, the worse its spectral resolution results. Welch suggested that a 50% overlap, with a cosine (Hanning) window, should be adopted, as it is carried out in current analysis. Concerning the effective bandwidth, for Welch's method, it can be expressed as $\Delta f_e = \alpha_w T_0^{-1}$ where α_w is a factor that depends upon the kind of the selected taper and on the way bandwidth is defined. In the case of the Hanning window and considering a half-power bandwidth, we obtain $\alpha_w = 1.44$. Concerning the variance of the estimator, with a 50% overlap, a relative standard uncertainty (standard deviation) $u_S(f)/S(f) = \sqrt{(11/18)N_0N^{-1}}$ can be assumed, where $S(f)$ is the PSD and

$u_S(f)$ is the absolute standard uncertainty. An example of the application of design of the estimator will be provided in the next subsection.

Let us now briefly consider Thomson's multitaper approach. Basically, this method generalizes the tapering issue by adopting multiple orthogonal tapers, with the aim of recovering information that may be lost when using a single taper. The estimator is the average of K direct spectral estimators, each acting on the whole data record (rather than on a signal segment, as happens in Welch method) and applying a different taper. Each (partial) estimator is defined by:

$$\hat{S}_k(f) = \Delta t \left| \sum_{i=1}^{N} h_{i,k} x_{i+l-1} e^{-j2\pi fi\Delta t} \right|^2 \tag{7.8}$$

where $h_{i,k}$ is the k th data taper, usually chosen as the k th discrete prolate spheroidal sequence with parameter W, where $2W$ is the normalized bandwidth of the tapers, i.e., the bandwidth for $\Delta t = 1$ s. The final estimator is thus:

$$\hat{S}(f) = \frac{1}{K} \sum_{k=0}^{K-1} \hat{S}_k(f) \tag{7.9}$$

where K is typically chosen to be equal to $2NW - 1$. The metrological characteristics of the procedure can be kept under control by assuming an effective bandwidth $\Delta f_e = 2W/\Delta t$ (Hz) and considering that the estimator is approximately equal in distribution to $S(f)\chi^2_{2K}/2K$, which yields a relative standard uncertainty equal to $K^{-\frac{1}{2}}$. Therefore, with respect to Welch method, there is here much less arbitrariness, since, for a fixed observation time, T, the only parameter to be chosen is the half-bandwidth W, which influences both spectral resolution and relative standard uncertainty. Again, examples of application will be provided in the next section.

7.2.2 *Spectral Analysis of Simulated Sea Wave Measurement Data*

The performance of different methods of spectrum estimation can be compared by simulating observations, i.e., signals, from a given PSD, and applying to them and comparing the results, keeping the assumed spectrum as the reference one. Form a metrological standpoint, spectrum measurement can be seen as a kind of indirect dynamic measurement, developed in two steps: the measurement of the time history of the phenomenon and the processing of the acquired signal by a spectrum estimation procedure [15]. Dynamic calibration of the overall measurement process is often quite difficult. Therefore, it makes sense to calibrate the two parts separately. In this perspective, assessing the performance of the spectrum estimator by simulated signals of the same kind as those that are likely to be encountered in actual application may be seen as a (partial) dynamic calibration.

To illustrate this procedure, signals from both the single-peak spectrum of Fig. 7.1a [16] and the double-peak spectrum of Fig. 7.1b, were generated, assuming a sampling rate of $f_s = 2.0$ Hz [17], and a total duration $T = 3600\ s$, and both Welch's and Thomson's spectra were calculated. For doing that, the design considerations presented above must be applied. In the case of the single-peak spectrum, an optimum trade-off between spectral resolution and relative uncertainty of the spectrum estimate was reached by assuming a duration of the observation window, $T_0 = 120$ s = 2 min, which corresponds to an effective bandwidth $\Delta f_e = 0.012$ Hz and to a relative standard uncertainty $u_S(f)/S(f) = 0.14$. The resulting spectrum is presented in Fig. 7.3a. For applying the Thomson method, the same effective bandwidth was selected, which yielded a design parameter $NW = 21.6$, corresponding to a relative standard uncertainty $u_S(f)/S(f) = 0.15$. The corresponding spectrum is reported in Fig. Fig. 7.3b.

In the case of the double-peak spectrum, a better spectral resolution is required, for the presence of peaky swell component. Therefore, with Welch's method, a larger observation duration was selected, namely $T_0 = 360\ s = 6\ min$, corresponding to an effective bandwidth $\Delta f_e = 0.0o4\ Hz$ and to a relative standard uncertainty $u_S(f)/S(f) = 0.25$. The result is shown Fig. 7.1a.

Again, for the multitaper approach, the same effective bandwidth was selected, resulting in a design parameter $NW = 7.2$, corresponding to a relative standard uncertainty $u_S(f)/S(f) = 0.27$. The corresponding spectrum is reported in Fig. 7.4b.

It appears that both methods provide a consistent estimation of the spectra, yet Thomson method, despite its "noisy" appearance, provides a better reconstruction of the "shape" of the spectrum, which is what really matters. This is reflected also by the recovering of the sea state parameters, as it will be briefly outlined in the next subsection.

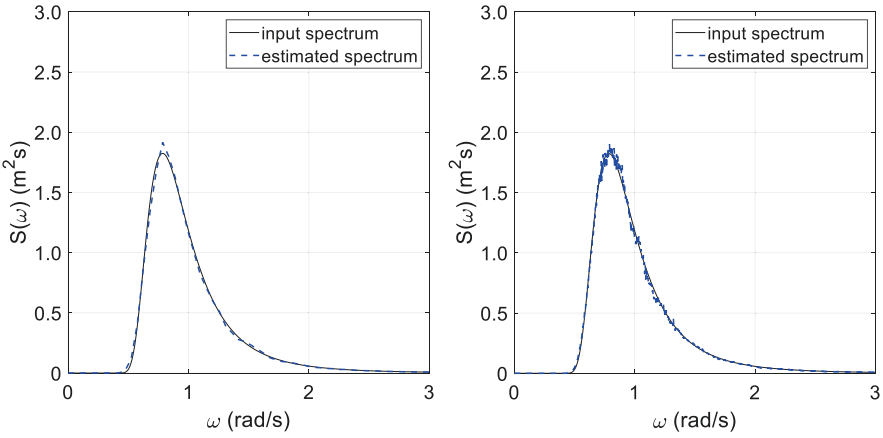

(a) Welch method (b) Thomson method

Fig. 7.3 Spectrum estimation of a signal generated from the spectrum of Fig. 7.1a: (**a**) Welch method, (**b**) Thomson method

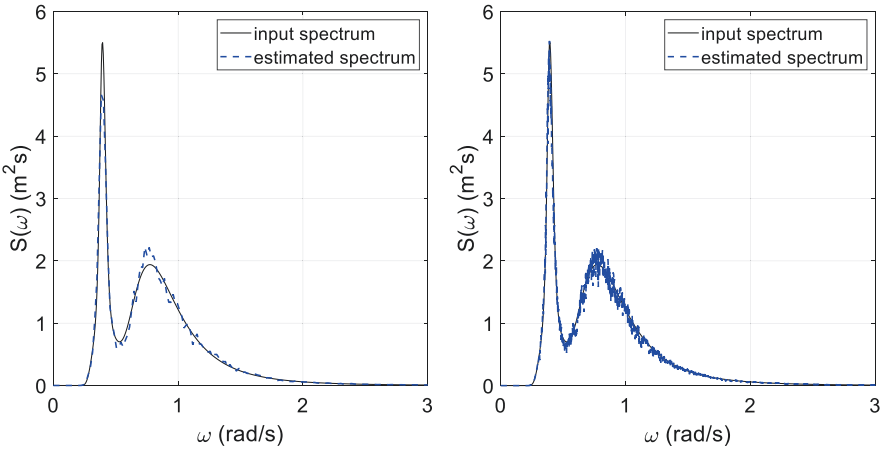

(a) Welch method (b) Thomson method

Fig. 7.4 Spectrum estimation of a signal generated from the spectrum of Fig. 7.1b: (**a**) Welch method, (**b**) Thomson method

7.2.3 Estimation of Sea State Parameters from Estimated Spectra

The sea state parameters, namely the significant wave height H_s, the wave peak period T_p, and the peak enhancement factor γ, are determined by the nonlinear least square method (NLSM), embodied by Rossi et al. [16] and generalized [17] to fit double-peak wave spectra, obtained by combined wind sea and swell components. In the general, bimodal case, the fitted wave spectrum is assessed by a two-step procedure. Firstly, the peak frequencies, corresponding to the swell and wind wave components, are preliminarily detected, as they correspond to the relative maxima of the smoothed estimated spectrum. Then, the remaining spectral parameters, namely the significant wave height and the peak enhancement factor of the two components, are obtained by the NLSM, based on the iterative trust-region-reflective algorithm and the interior-reflective Newton method [18]. Particularly, it allows detecting the unknown parameters by iteratively solving a large set of linear equations by the method of the preconditioned conjugate gradients.

The application of this method to the spectra presented in the previous subsection is presented in Tables 7.1 and 7.2.

It can be noted that both methods yield consistent estimations, yet Thomson methods prove to be more accurate, especially for the estimation of the peak enhancement factor of the swell component.

Table 7.1 Assessment of sea state parameters through the two spectrum estimation methods (JONSWAP)

Parameter	Input wave spectrum	Method	
		Welch	Thomson
H_s (m)	4.00	3.99	4.01
T_p (s)	8.00	8.00	7.94
γ	1.00	1.00	1.00

Table 7.2 Assessment of sea state parameters through the two spectrum estimation methods (bimodal)

Parameter	Input wave spectrum		Welch		Thomson	
	Wind wave	Swell	Wind wave	Swell	Wind wave	Swell
H_s (m)	4.00	3.00	4.01	2.99	4.01	2.95
T_p (s)	8.00	16.00	8.00	15.65	8.22	16.06
γ	1.00	5.00	1.00	4.00	1.00	4.77

7.3 Sea Wave Monitoring Based on Ship Motion Measurement and Analysis

7.3.1 A Brief Theoretical Review

A possible way to reliably monitor the sea waves is based on the measurement and analysis of ship motions in a seaway. This topic was widely investigated since the 70s when Takekuma and Takahashi [19] developed the first reverse analysis technique to detect the wave spectrum parameters based on the analysis of ship motions without forward speed. Subsequently, a variety of attempts were performed to include the ship speed and, consequently, the Doppler shift, for vessels advancing in head and bow seas [20, 21] and more recently in quartering and following seas [22]. Based on these pioneering works, in the last two decades, the interest of the scientific community on this research topic grew fast, as proved by the variety of research activities carried out throughout the world [23–26].

The wave spectrum resembling procedures are generally based on the frequency-domain analysis of ship motions, based on the following main assumptions [27]: (1) the ship motions are linear with the incident wave amplitude; (2) the incoming waves resemble an ergodic random process [28], so as all sea state parameters are stationary, in a stochastic sense, in a short time interval; and (3) the ship speed and course are kept constant during the ship motion measurements. Hence, the wave spectrum is subsequently detected by parametric or nonparametric modelling techniques. In the first case, the main sea states parameters are obtained assuming a priori a certain analytical formulation of the wave spectrum in order to subsequently detect the best-fit parameters. In the latter case, instead, the spectral shape is not specified a priori, and the wave spectrum is detected by the energy equivalence principle, so equating the 0th-order spectral moments of

the measured and resembled wave spectra. Only few attempts have been performed to detect the sea state parameters by time-domain techniques mainly based on Kalman filtering [29, 30], mainly due to the high numerical effort required to detect the unknown sea state parameters. In this case, in fact, the ship motion measurements are converted into the wave elevation time history, based on the ship response amplitude operators (RAOs) that, in any case, need to be preliminarily assessed in the frequency domain.

As concerns the selection of the ship motions embodied in the wave spectrum resembling procedure, different attempts and selections were embodied in the past, combining single and multiple motions with different weighting factors, in order to apply a robust sea state measuring procedure. Based on the main outcomes of past research activities, heave and pitch motions seem to be the most promising selection to detect the sea state parameters, eventually combined with sway [31] or roll [32] motions if the prevailing wave direction is not known a priori. In the following, the parametric procedure, recently developed by Piscopo et al. [28], is briefly discussed.

7.3.2 *Assessment of Sea State Parameters*

The sea state assessment procedure outlined in [28] is based on two subsequent steps. At the first step of the procedure, the wave peak period and the peak shape parameter are determined by an iterative procedure that allows detecting the best-fit parameters of the JONSWAP spectrum, as depicted in Fig. 7.5.

Particularly, at the first step the heave S_{ξ_3} and pitch motion S_{ξ_5} motion spectra are preliminarily assessed in the encounter frequency domain ω_e by spectral analysis of ship motions recorded by the onboard measuring equipment. In this respect, the heading angle between the vessel route and the prevailing sea waves is obtained by independent systems, such as wave radars. Hence, the unknown wave spectrum parameters, namely the wave peak period and the peak shape parameter, are iteratively varied to maximize the following parameter:

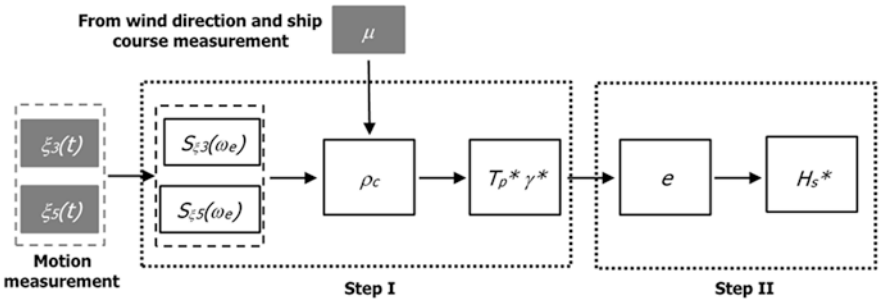

Fig. 7.5 Flow chart of the two-step iterative procedure [28], reprinted by permission

$$\varrho_c\left(T_p^i,\gamma^j\right)=\sqrt{\sum_{k=3,5}\left[\rho\left(\frac{S_{\xi_k}\left(\boldsymbol{\omega_e}\right)}{\int_0^\infty S_{\xi_k}\left(\omega_e\right)d\omega_e},\frac{\left|H_k\left(\boldsymbol{\omega_e}\right)\right|^2 S_J\left(H_s,T_p^i,\gamma^j,\boldsymbol{\omega_e}\right)}{\int_0^\infty\left|H_k\left(\omega_e\right)\right|^2 S_J\left(H_s,T_p^i,\gamma^j,\omega_e\right)d\omega_e}\right)\right]^2} \tag{7.10}$$

having denoted by ρ the Pearson correlation coefficient and by H_k the complex ship motion transfer function for heave (3) and pitch (5) motions. At the second step of the procedure, the significant wave height is assessed based on single or combined heave and pitch motion:

$$H_s^*=\begin{cases}\dfrac{\xi_{5,s}}{4\sqrt{\int_0^\infty\left|H_5\left(\omega_e\right)\right|^2 S_J\left(1,T_p^*,\gamma^*,\omega_e\right)d\omega_e}} \; if\; e\le 1/2\\ \sqrt{\prod_{k=3,5}\dfrac{\xi_{k,s}}{4\sqrt{\int_0^\infty\left|H_k\left(\omega_e\right)\right|^2 S_J\left(1,T_p^*,\gamma^*,\omega_e\right)d\omega_e}}} \; if\; 1/2<e<2\\ \dfrac{\xi_{3,s}}{4\sqrt{\int_0^\infty\left|H_3\left(\omega_e\right)\right|^2 S_J\left(1,T_p^*,\gamma^*,\omega_e\right)d\omega_e}} \; if\; e\ge 2\end{cases} \tag{7.11}$$

having denoted by e the ship kinetic parameter:

$$e=\frac{\left(\Delta+A_{33,\infty}\right)\ddot{\xi}_{3,s}^2}{\left(I_{55}+A_{55,\infty}\right)\ddot{\xi}_{5,s}^2} \tag{7.12}$$

In Eq. (7.12), Δ (I_{55}) denotes the ship displacement (pitch moment of inertia), $A_{33,\infty}$ ($A_{55,\infty}$) is the heave (pitch) added mass at infinite frequency and $\ddot{\xi}_{3,s}$ ($\ddot{\xi}_{5,s}$) is the heave (pitch) motion significant velocity, as obtained by the onboard measurements.

7.3.3 Assessment of Sea State Parameters

The procedure outlined in Subsect. 7.3.2 allows efficiently measuring the sea state parameters of single peaked wave spectra, as proved by the numerical investigation reported in the benchmark study performed by Piscopo et al. [28] with reference to the well-known S175 containership [33, 34]. Particularly, the heave and pitch motion time histories, obtained by time-domain simulations after solving the relevant coupled nonlinear equations, were subsequently embodied as input for the two-step procedure. In this respect, Figs. 7.4 and 7.5 report a comparative analysis between the input and resembled parameters for a fully developed sea with 3.0 m

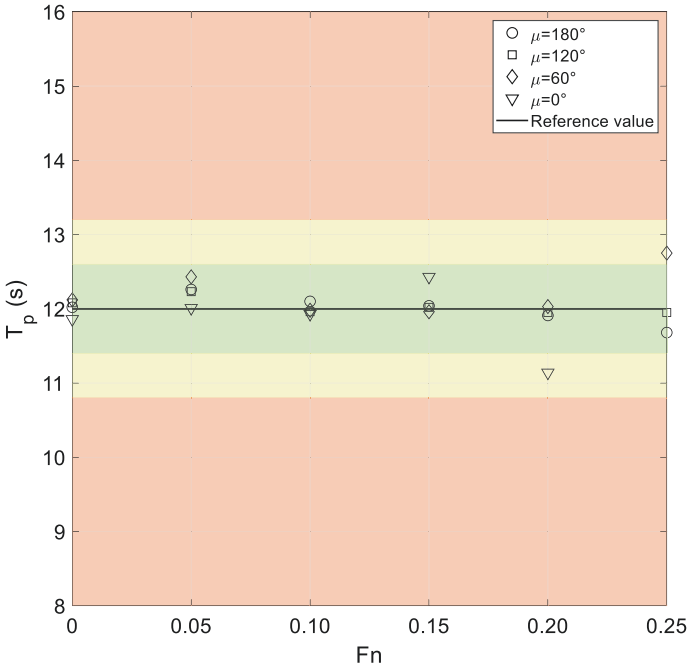

Fig. 7.6 Assessment of the wave peak period [28], reprinted by permission

wave height and 12.0 s peak period, at different vessel speeds corresponding to a Froude number (Fn) ranging from 0 up to 0.25. The green area represents the set of values with a percentage error, as regards the reference one, less than 5%, while the yellow and red areas refer to percentage errors up to and beyond 10%, respectively. As it can be gathered from Figs. 7.6 and 7.7, the resembled values of the wave peak period and significant wave height almost always lie in the green area, so proving the effectiveness of the proposed procedure.

7.4 Sea Wave Monitoring by Coastal HF Radars

Over the last decades, HF (high-frequency) radars (3–50 MHz) have been increasingly used for monitoring the surface current field in coastal areas, with a wide spectrum of applications ranging from maritime safety to coastal zone management, including operational purposes such as oil spill response and pollution assessment [35]. The functioning principles of coastal HF radars are very briefly described in chap. 9 of this same volume [36]. As explained in [36], HF radar signals are backscattered by the sea surface roughness induced by the presence of gravity waves [37]. In presence of Bragg scattering, the backscattered signal yields a Doppler shift owing to the underlying currents [38]; these are the strongest signals reflected by the

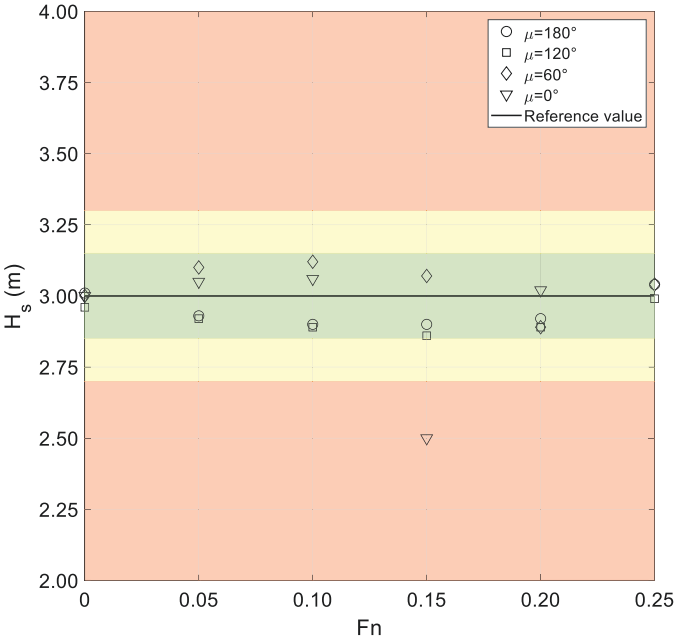

Fig. 7.7 Assessment of the significant wave height [28], reprinted by permission

sea surface, the first-order echoes, which provide information on the surface current field. Nonlinear wave interactions and double scattering processes [39], on the other hand, give rise to second-order echo spectra, the source of information on surface waves (see Fig. 7.8) [41–44]. identified a relationship between the HF backscattered Doppler spectrum and the ocean wave directional spectrum, thus enabling to derive wave height and dominant wave period from HF radar data. Stemming from this result, several techniques have been developed to reconstruct the wave directional spectrum from HF data (see [45] for a review of early reconstruction methods; [46] for a recent summary of inversion techniques).

Thus, HF radars have the potential of measuring the surface wave field by proper analysis of the second-order echoes. This peculiarity makes them ideal platforms for the study of a wide range of processes in coastal areas, including year-long monitoring of coastal basins [46, 47], sea storms [48], or tsunamis [49]. It is worth underlining that, differently from other systems that give single-point information (e.g., wave buoys, ADCPs), HF radars provide measurements of surface gravity waves over larger areas of the basin of interest, thus allowing for a more accurate description of the development of the wave field.

Despite such a great potential, wave retrieval from HF radars has received less attention compared to surface current measurements [46]. This is mostly due to inherent technical limitations. Second-order spectra are much less straightforward to handle than first-order ones, as they are typically much weaker and often disturbed, at least partly, by the measurement noise. This occurs, in particular, in the

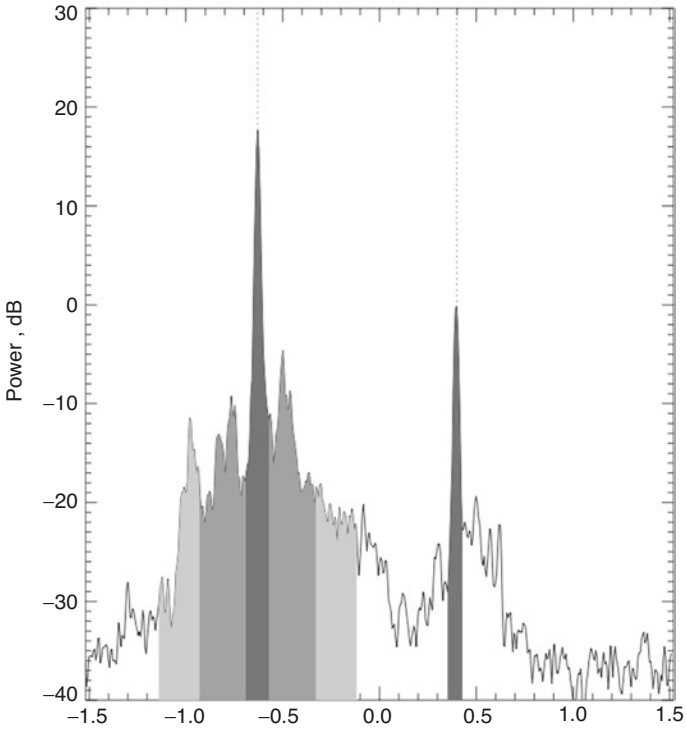

Fig. 7.8 Example of a typical low sea state Doppler spectrum measured by a coastal HF radar. Dark grey: first-order Bragg peaks, used for surface current estimation (theoretical positions shown with dotted lines); medium grey: second-order spectrum used for significant wave height and directional spectrum estimation; light grey: additional part of the second-order spectrum used in mean period estimation. From [40], reprinted by permission

case of intense surface currents: in this case, the first-order peaks may mask at least in part the second-order ones. Moreover, limits to the minimum and maximum detectable wave heights exist. The former is due to the low signal-to-noise ratio in case of low sea state conditions; the latter is due to the fact that the maximum detectable wave height depends on the radar frequency as follows [39, 50–52]:

$$h_{sat} = \frac{2}{k_0}[m] \tag{7.13}$$

where k_0 is the radar wavenumber, yielding an underestimation or overestimation of wave heights above h_{sat}. It is worth noticing that this upper limit decreases in shallow water conditions.

However, even though in the awareness of the above caveats, the use of HF radars to estimate surface wave parameters is becoming more and more widespread as this kind of instruments has started to be clustered in local and larger-scale networks

[36], even though we are still far from being able to deliver HF radar-derived wave data on an operational basis (even though steps are being taken in this direction: see [53, 54]). Such measurements have been carried out so far in various coastal areas of the world ocean, spanning from California to New Jersey, from northwestern Spain to the British and Irish coasts, to Norway, and in the Mediterranean in the Malta–Sicily Channel and in the Gulf of Naples [55–64]. On the northern coast of Cornwall, UK, a specific HF radar site has been installed expressly to measure waves in a test site for offshore renewable energy studies (the Wave Hub, [39]).

Obviously, in order to provide reliable data, measurements must be validated; this is always true, but assumes a special importance in the case of remotely sensed data. This is routinely carried out for all HF radar installations. In particular, for wave observations, this has been done by comparing HF radar data with wave buoy measurements, ADCPs and/or with wave model outputs [39, 52, 61, 64].

HF radars can be roughly divided into two categories: direction-finding and beam-forming (or phased array, for a recent assessment of the performance of both kinds of systems see [65]). In order to exemplify the potential of a coastal HF radar for measuring waves, we will look at results obtained with systems belonging to the first group, and in particular with SeaSonde ones, manufactured by CODAR Ocean Sensors (where CODAR originally stands for Coastal Ocean Dynamics Applications Radar [66]), which are compact radars that compare phases and amplitudes of back-transmitted signals using direction-finding inversion algorithms. In such systems, as explained, e.g., by [52], wave spectra are derived from HF radar data fitting them to a locally optimized Pierson–Moskowitz spectrum (see above, Sect. 7.1.2). This allows to indirectly derive directional and nondirectional wave parameters such as significant wave height, centroid period, and direction. In SeaSonde radars, these parameters are averaged along evenly distributed annuli (range cells, RCs) centred on the antenna. RCs spacing depends on the operating frequency of the radars, ranging from 5 km for long-range systems (5 MHz) [52] to 1 km for short-range ones (25 MHz) [46]. This feature allows the reconstruction of the wave field along a radial transect, permitting the evaluation of the coast-offshore changes in the parameters. In the following, the characterization of the wave field in two different environments is illustrated, with the aim of highlighting the potentialities of these systems and their possibilities of improvement.

The Gulf of Naples (Tyrrhenian Sea) is site to the oldest, presently running European HF radar network, managed by the Department of Science and Technology of the Parthenope University [67]. Over the years, this system has been exploited to reconstruct seasonal circulation patterns and transport dynamics [68–71]. In recent times, its potential use in wave retrieval has been investigated as well [40, 46, 53, 64]. The HF radar-derived measurements have been compared with historical data from the Gulf of Naples [46] and with model results [64], returning good consistency among the different platforms. Annual [46, 53] and interannual [47] investigations allowed the identification of specific seasonal patterns, linking the wave field characteristics to the prevailing meteorological forcing acting over the area, as well as illustrating specific directional prevalence in different subsectors of the basin.

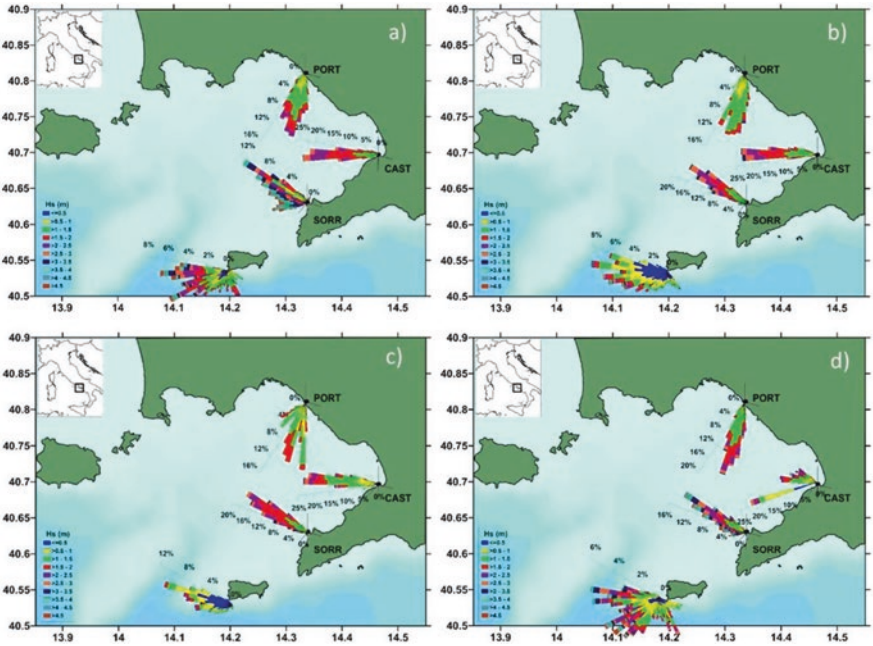

Fig. 7.9 Seasonal rose diagrams of significant wave heights for the year 2010 measured in the Gulf of Naples by three HF radar stations (Portici, Castellamare, and Sorrento, from north to south) and by a wave buoy off the island of Capri (farthest south): (**a**) winter, (**b**) spring, (**c**) summer, (**d**) autumn. From [46], redrawn by permission

This can be seen in Fig. 7.9, where seasonal rose diagrams of significant wave height for the whole year 2010 are shown along with in situ wave buoy measurements collected off the Island of Capri. The radar system was composed of three short-range 25 MHz transceiving stations, whose measurements showed a site-dependent pattern: provenance recorded at RC 5 (5 km from the station) was fairly constant for each site (including the wave buoy location) but different from one site to another, thus underlining the ability of the HF radar observations to resolve the spatial variability of the wave field over even such a small basin.

Another example of utilization of wave data from HF radars in the framework of a synoptic multiplatform wave regime observation network is shown in Fig. 7.10. The map displays wave and wind observations gathered along the Galician coast (NW Spain) over approximately 16 months (January 2014–April 2015). Waves were measured at RC 2 (10 km from the stations) by two long-range HF systems transmitting at 5 MHz approximately (SILL and VILA on the map), two wave buoys (SB and VB on the map), estimated in three points with a model (SO2, S20 and S24 on the map), while wind data were collected by two weather stations (CW on land, VBW on the VB buoy). Also in this case, the results returned robust validations and the HF radar-derived measurements improved the knowledge of the wave field dynamics in a particularly energetic area of the coastal eastern Atlantic Ocean.

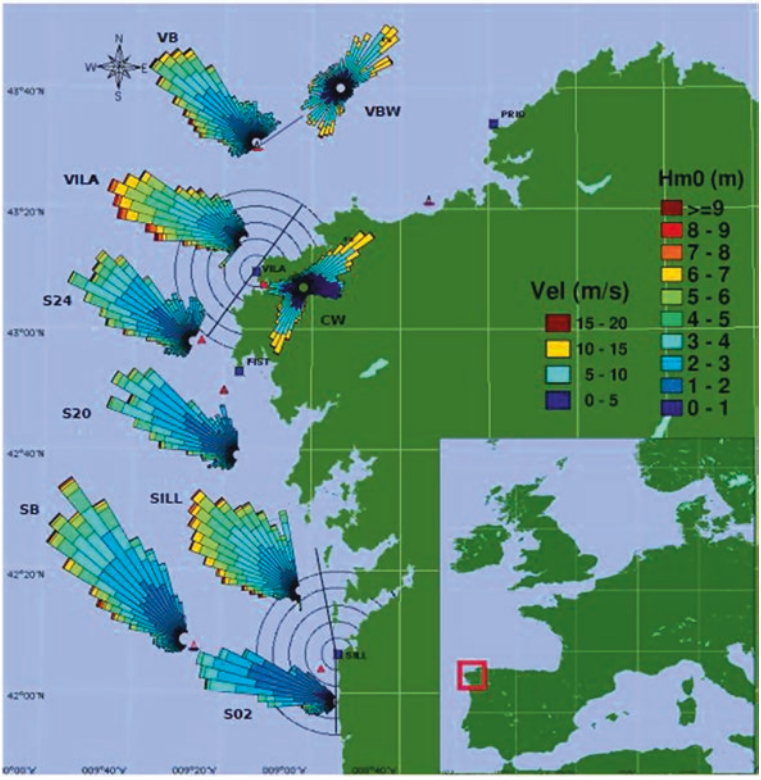

Fig. 7.10 Rose diagrams of significant wave heights for the period January 2014–April 2015 measured off the northwestern coast of Galicia by two HF radar stations (VILA = Vilàn and SILL = Silleiro), two wave buoys (VB and SB), estimated in three sites by a numerical model (S24, S20 and S02), along with wind roses measured by two weather stations (CW on land, VBW on the VB buoy). From [52], reprinted by permission

7.5 Future Developments

The applied advanced sea spectrum reconstruction methods seem to be promising for future developments, mainly related to: (1) reduce the time duration of the wave history, without penalizing the effectiveness of the sea spectrum reconstruction method, and (2) extend the above-mentioned techniques to the sea spectrum reconstruction methods, based on onboard ship motion measurement and analysis. Finally, the positive results gathered over the last years have demonstrated that HF radars can realistically retrieve surface wave parameters in different environments. As discussed in [46], the functioning and performance of these systems need some future improvement and refinement, such as standardization of QA/QC protocols, and optimization of inversion methods and of wave retrieval algorithms. Nonetheless, HF radars can potentially qualify as effective operational tools [72], supporting and integrating already existing observation networks.

References

1. Lewis E (1989) Principles of naval architecture—volume III: motions in waves and controllability. Society of Naval Architects and Marine Engineers, NJ
2. Chakrabarti SK (2005) Handbook of offshore engineering. Elsevier, Amsterdam
3. Det Norske Veritas (2010) Environmental conditions and environmental loads. Recommended Practice DNV-RP-C205
4. Neumann G (1953) On ocean wave spectra and a new method of forecasting wind-generated sea. In: Technical memory 43. Beach Erosion Board, US Army Corp of Engineers, Washington
5. Roll H, Fischer G (1956) Eine Kritische Bemenkung Zum Neumann-Spektrum der Seeganger. Deutsche Hydrografische Zeitschrift 9:9–14
6. Darbyshire J (1957) Eine Bemerkung über den Vergleich von Formeln verschiedener Autoren zur Berechnung von Wellenspektren. Deutsche Hydrografische Zeitschrift 10:184–190
7. Pierson WJ, Moskowitz L (1964) A proposed spectral form for fully developed wind seas based on the similarity theory of S.A. Kitaigorodski. J Geophys Res 69(24):5181–5190
8. Ochi MK, Hubble EN (1976) On six-parameters wave spectra. In: Proceedings of the 15th coastal engineering conference, Honolulu, Hawaii, pp. 301–328
9. Torsethaugen K, Haver S (2004) Simplified double peak spectral model for ocean waves. In: Proceedings of the 14th international offshore and polar engineering conference, Toulon
10. Percival DB, Walden AT (2020) Spectral analysis for univariate time series. Cambridge University Press, Cambridge
11. Schuster A (1898) On the investigation of hidden periodicities with application to a supposed 26 Day period of meteorological phenomena. Terr Magn 3:13–41
12. Welch PD (1967) The use of fast Fourier transform for the estimation of power spectra: a method based on time averaging over short modified periodograms. IEEE Trans Audio Electroacoust 15:70–73
13. Thomson DJ (1982) Spectrum estimation and harmonic analysis. Proc IEEE 70:1055–1096
14. Marple SL (1987) Digital spectral analysis. Prentice—Hall, Englewood Cliffs
15. Rossi GB (2012) Towards an Interdisciplinary Probabilistic Theory of Measurement. IEEE Trans. Instrum. Meas. 61(8):2095-2106
16. Rossi GB, Crenna F, Piscopo V, Scamardella A (2020) Comparison of spectrum estimation methods for the accurate evaluation of sea state parameters. Sensors 20:1416
17. Rossi GB, Crenna F, Berardengo M, Piscopo V, Scamardella A (2020) In: Proc. 2020 IMEKO TC-19 international workshop on metrology for the sea, Naples, Italy, October 5–7
18. Coleman TF, Li Y (1996) Trust region approach for nonlinear minimization subject to bounds. SIAM J Optim 6:418–445
19. Takekuma K, Takahashi T (1973) On the evaluation of sea spectra based on the measured ship motions. Trans West-Japan Soc Naval Arch 45:51–57
20. Isobe M, Kondo K, Horikawa K (1984) Extension of MLM for estimating direction wave spectrum. In: Proceedings of the symposium on description and modeling of direction seas, volume A-6
21. Kobune K, Hashimoto N (1986) Estimation of directional spectra from the maximum entropy principle. In: Proceedings of the 5th international offshore mechanics and Arctic engineering (OMAE) symposium, Tokyo, pp. 80–85
22. Iseki T, Ohtsu K (2000) Bayesian estimation of directional wave spectra based on ship motions. Control Eng Pract 8:215–219
23. Iseki T, Terada D (2002) Bayesian estimation of direction wave spectra for ship guidance systems. Int J Offshore Polar Eng 12:25–30
24. Nielsen UD (2006) Estimations of on-site direction wave spectra from measured ship responses. Mar Struct 19:33–69
25. Nielsen UD, Andersen IMV, Koning J (2013) Comparisons of means for estimating sea states from an advancing large containership. In: Proceedings of the 12th PRADS, Changwon, South Korea

26. Montazeri N, Nielsen UD, Jensen JJ (2016) Estimation of wind sea and swell using shipboard measurements – a refined parametric modelling approach. Appl Ocean Res 54:73–86
27. Ochi MK (1990) Applied probability and stochastic processes in engineering and physical sciences. Wiley, New York
28. Piscopo V, Scamardella A, Gaglione S (2020) A new wave spectrum resembling procedure based on ship motion analysis. Ocean Eng 201:107137
29. Pascoal R, Guedes Soares C (2009) Kalman filtering of vessel motions for ocean wave directional spectrum estimation. Ocean Eng 36:477–488
30. Pascoal R, Perera LP, Guedes Soares C (2017) Estimation of directional spectra from ship motions sea trials. Ocean Eng 132:126–137
31. Tannuri EA, Sparano JV, Simos AN, Da Cruz JJ (2003) Estimating directional wave Spectrum based on stationary ship motion measurements. Appl Ocean Res 25:243–261
32. Nielsen UD (2006) Estimations of on-site direction wave spectra from measured ship responses. Mar Struct 19:33–69
33. ITTC (1978) Report of the seakeeping committee. In: Proceedings of the 15th international towing tank conference, the Hague, 1, 55–114
34. Kim M, Hizir O, Turan O, Day S, Incecik A (2017) Estimation of added resistance and ship speed loss in a seaway. Ocean Eng 141:465–476
35. Paduan JD, Washburn L (2013) High-frequency radar observations of ocean surface currents. Ann Rev Mar Sci 5:115–136. https://doi.org/10.1146/annurev-marine-121211-172315
36. Ferla M, Nardone G, Orasi A, Picone M, Falco P, Zambianchi E (2021) Sea-monitoring networks
37. Crombie DD (1955) Doppler spectrum of sea echo at 13.56 Mc/ s. Nature 175:681–682
38. Barrick DE, Evans MW, Weber BL (1977) Ocean surface currents mapped by radar. Science 198:138–144
39. Lopez G, Conley DC, Greaves D (2016) Calibration, validation, and analysis of an empirical algorithm for the retrieval of wave spectra from HF radar sea echo. J Atmos Oceanic Tech 33(2):245–261
40. Wyatt LR (2002) An evaluation of wave parameters measured using a single HF radar system. Can J Remote Sens 28(2):205–218
41. Barrick DE (1972a) First-order theory and analysis of MF/HF/VHF scatter from the sea. IEEE Trans Antennas Propag 20:2–10
42. Barrick DE (1972b) Remote sensing of sea state by radar. In: Derr VE (ed) Remote sensing of the troposphere. GPO, Washington
43. Barrick DE (1977a) Extraction of wave parameters from measured HF radar sea-echo Doppler spectra. Radio Sci 12:415–424
44. Barrick DE, Weber BL (1977) On the nonlinear theory for gravity waves on the ocean's surface. Part II: interpretation and applications. J Phys Oceanogr 7:11–21
45. Wyatt L (1986) The measurement of the ocean wave directional spectrum from HF radar Doppler spectra. Radio Sci 21:473–485
46. Saviano S, Kalampokis A, Zambianchi E, Uttieri M (2019) A year-long assessment of wave measurements retrieved from an HF radar network in the Gulf of Naples (Tyrrhenian Sea, Western Mediterranean Sea). J Operat Oceanogr 12(1):1–15
47. Saviano S, Cianelli D, Zambianchi E, Conversano F, Uttieri M (2020) An integrated reconstruction of the multiannual wave pattern in the Gulf of Naples (south-eastern Tyrrhenian Sea, Western Mediterranean Sea). J Marine Sci Eng 8(5):372
48. Lipa B, Barrick D, Alonso-Martirena A, Fernandes M, Ferrer MI, Nyden B (2014) Brahan project high frequency radar ocean measurements: currents, winds, waves and their interactions. Remote Sens (Basel) 6:12094–12117
49. Lipa BJ, Barrick DE, Bourg J, Nyden BB (2006) HF radar detection of tsunamis. J Oceanogr 62:705–716
50. Lipa BJ, Barrick D, Isaacson J, Lilleboe PM (1990) CODAR wave measurements from a north sea semisubmersible. IEEE J Ocean Eng 15:119–125

51. Wyatt LR, Green JJ (2009) Measuring high and low waves with HF radar, OCEANS 2009-EUROPE. IEEE Bremen 1:1–5
52. Basañez A, Lorente P, Montero P, Álvarez-Fanjul E, Pérez-Muñuzuri V (2020) Quality assessment and practical interpretation of the wave parameters estimated by HF radars in NW Spain. Remote Sens (Basel) 12(4):598
53. Falco P, Buonocore B, Cianelli D, De Luca L, Giordano A, Iermano I et al (2016) Dynamics and sea state in the Gulf of Naples: potential use of high-frequency radar data in an operational oceanographic context. Jf Operat Oceanogr 9:33–45
54. Lorente P, Varela SP, Soto-Navarro J, Ruiz MI, Álvarez-Fanjul E, Montero P (2016) The high-frequency coastal radar network operated by Puertos del Estado (Spain): Roadmap to a fully operational implementation. IEEE J. Ocean. Eng. 42(1):56-72.
55. Long RM, Barrick D, Largier JL, Garfield N (2011) Wave observations from Central California: SeaSonde systems and in situ wave buoys. J Sens 2011
56. Beckenbach E, Washburn L (2004) Low-frequency waves in the Santa Barbara Channel observed by high-frequency radar. J Geophys Res Oceans 109:2
57. Kohut J, Roarty H, Licthenwalner S, Glenn S, Barrick D, Lipa B, Allen A (2008) Surface current and wave validation of a nested regional HF radar network in the mid-Atlantic bight. In: 2008 IEEE/OES 9th working conference on current measurement technology, IEEE, pp. 203-207
58. Lorente P, Sotillo MG, Aouf L, Amo-Baladrón A, Barrera E, Dalphinet A et al (2018) Extreme wave height events in NW Spain: a combined multi-sensor and model approach. Remote Sens (Basel) 10(1):1
59. Lorente P, Basañez Mercader A, Piedracoba S, Pérez-Muñuzuri V, Montero P, Sotillo MG, Álvarez-Fanjul E (2019) Long-term skill assessment of SeaSonde radar-derived wave parameters in the Galician coast (NW Spain). Int J Remote Sens 10:9208–9236
60. Wyatt LR, Green JJ (2009) Measuring high and low waves with HF radar, OCEANS 2009-EUROPE. IEEE Bremen 1:1–5
61. Wyatt LR, Green JJ, Gurgel KW, Borge JN, Reichert K, Hessner K, Reistad M (2003) Validation and intercomparisons of wave measurements and models during the EuroROSE experiments. Coastal Eng 48(1):1–28
62. Atan R, Goggins J, Hartnett M, Nash S, Agostinho P Assessment of extreme wave height events in galway bay using high frequency radar (CODAR) Data. In: Proceedings of the 1st international conference on renewable energies offshore (RENEW), Lisbon, 24–26 November 2014
63. Orasi A, Picone M, Drago A, Capodici F, Gauci A, Nardone G et al (2018) HF radar for wind waves measurements in the Malta-Sicily Channel. Measurement 128:446–454
64. Saviano S, De Leo F, Besio G, Zambianchi E, Uttieri M (2020) HF radar measurements of surface waves in the Gulf of Naples (southeastern Tyrrhenian Sea): comparison with hindcast results at different scales. Front Mar Sci
65. Hardman RL, Wyatt LR, Engleback CC (2020) Measuring the directional ocean spectrum from simulated bistatic HF radar data. Remote Sens (Basel) 12(2):313
66. Barrick DE, Lipa BJ (1985) Mapping surface currents. Sea Technol 26:43–48
67. Rubio A, Mader J, Corgnati L, Mantovani C, Griffa A, Novellino A et al (2017) HF radar activity in European coastal seas: next steps toward a pan-European HF radar network. Front Mar Sci 4:8
68. Uttieri M, Cianelli D, Nardelli BB, Buonocore B, Falco P, Colella S, Zambianchi E (2011) Multiplatform observation of the surface circulation in the Gulf of Naples (southern Tyrrhenian Sea). Ocean Dyn 61(6):779–796
69. Cianelli D, Falco P, Iermano I, Mozzillo P, Uttieri M, Buonocore B et al (2015) Inshore/offshore water exchange in the Gulf of Naples. J Mar Syst 145:37–52
70. Iermano I, Moore AM, Zambianchi E (2016) Impacts of a 4-dimensional variational data assimilation in a coastal ocean model of southern Tyrrhenian Sea. J Mar Syst 154:157–171

71. Cianelli D, D'Alelio D, Uttieri M, Sarno D, Zingone A, Zambianchi E, d'Alcalà MR (2017) Disentangling physical and biological drivers of phytoplankton dynamics in a coastal system. Sci Rep 7(1):1–15
72. Wyatt LR, Thompson SP, Burton RR (1999) Evaluation of high frequency radar wave measurement. Coast Eng 37(3–4):259–282
73. Hasselmann K, Barnet TP, Bouws E, Carlson H, Cartwright DE, Enke K, Ewing JA, Gienapp H, Hasselman DE, Kruseman P, Meerburg A, Müller P, Olbers DJ, Richter K, Sell W, Walden H (1973) Measurements of wind-wave growth and swell decay during the joint North Sea wave project (JONSWAP). Deutschen hydro-graphischen Institut, Hamburg
74. Fonseca N, Guedes Soares C (1998) Time-domain analysis of large amplitude vertical ship motions and wave loads. J Ship Res 42(2):139–153